ACS APPLIED MATERIALS & INTERFACES

Research Article

www.acsami.org

Predictive Model for the Design of Zwitterionic Polymer Brushes: A Statistical Design of Experiments Approach

Ramya Kumar[†,∥] and Joerg Lahann*[,†,‡,§,⊥,∥]

[†]Department of Chemical Engineering, [‡]Department of Macromolecular Science & Engineering, [§]Department of Material Science & Engineering, [⊥]Department of Biomedical Engineering, and [∥]Biointerfaces Institute, University of Michigan, Ann Arbor, Michigan 48109, United States

Supporting Information

ABSTRACT: The performance of polymer interfaces in biology is governed by a wide spectrum of interfacial properties. With the ultimate goal of identifying design parameters for stem cell culture coatings, we developed a statistical model that describes the dependence of brush properties on surface-initiated polymerization (SIP) parameters. Employing a design of experiments (DOE) approach, we identified operating boundaries within which four gel architecture regimes can be realized, including a new regime of associated brushes in thin films. Our statistical model can accurately predict the brush thickness and the degree of intermolecular association of poly[{2-(methacryloyloxy) ethyl} dimethyl-(3-sulfopropyl) ammonium hydroxide] (PMEDSAH), a previously reported synthetic substrate for feeder-free and xeno-free culture of human embryonic stem cells. DOE-based multifunctional predictions offer a powerful quantitative framework for designing polymer interfaces. For example, model predictions can be used to decrease the critical thickness at which the wettability transition occurs by simply increasing the catalyst quantity from 1 to 3 mol %.

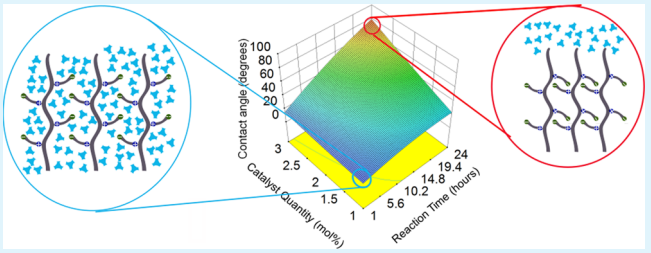

KEYWORDS: *PMEDSAH, stem cell culture, zwitterionic self-association, response surface methodology, surface-initiated atom transfer radical polymerization*

1. INTRODUCTION

The performance of responsive polymer brushes,[1−6] antifouling coatings,[7] antimicrobial coatings,[8,9] biosensor coatings,[10] or substrates for regenerative medicine is defined by the subtle interplay of interfacial properties such as thickness, wettability, swelling ratio, friction coefficient, roughness, or surface charge.[5,11,12] In the case of polymer brushes, these properties are readily modified by varying the brush composition, i.e., by choosing a suitable monomer, as well as by varying the brush architecture. Recent advances in controlled radical polymerization techniques (CRP), such as surface-initiated nitroxide-mediated polymerization[13] (SI-NMP), surface-initiated reversible addition−fragmentation transfer[14,15] (SI-RAFT) polymerization, and surface-initiated atom transfer radical polymerization[16] (SI-ATRP), have enabled the creation of tailored polymer brushes of desired architectures. CRP, when used to grow polymer brushes from substrate-bound initiators, has far-ranging possibilities, with a vast and steadily expanding library of monomers, initiator systems, substrate choices, and polymer architectures.[17−19] Compared to other CRP techniques, SI-ATRP is compatible with a wider range of functional monomers, more tolerant of impurities, and easier to access experimentally.

The selection of optimal SI-ATRP conditions is a critical element in polymer brush design, because the resultant brush properties are influenced by several experimental parameters and sometimes even combinations of SI-ATRP parameters.[20,21] The traditional iterative approach that relies on one-factor-at-a-time[22] optimization of polymerization recipe is inefficient and time-consuming. High-throughput combinatorial approaches[23] and computer-aided methods[24] for screening and optimizing solution ATRP conditions have been proposed, but it is unclear whether these will be effective when translated to SI-ATRP. A recent study tried to address this issue by developing a photonic microring resonator for real time monitoring[25] of brush growth, but data interpretation remains difficult.

Properties of polymer brushes prepared by surface-initiated polymerization (SIP) have been predicted using a combination of experimental investigations and mathematical models.[26] Kinetic modeling and simulations have been employed successfully to predict polymer film thickness as a function of time.[27,28] In predicting the kinetic trajectory for certain polymerization conditions, these studies have also provided mechanistic insights on the nature of initiation, chain transfer, propagation and termination[29] in SI-ATRP. However, the development of these mathematical models requires prior knowledge of the rate constants as well as experimental determination of the chain length distribution (CLD) of

Received: April 13, 2016
Accepted: June 7, 2016

DOI: 10.1021/acsami.6b04370
ACS Appl. Mater. Interfaces XXXX, XXX, XXX−XXX

Table 1. Experimental Space Constructed for Statistical Model Development[a]

factor	coding	numberof levels	units	factor levels studied				
catalyst quantity [CuCl]:[Monomer]	A	3	mol %	1%	2%	3%		
catalyst ratio [CuCl]:[$CuCl_2$]	B	3		2.5	5	10		
reaction time	C	5	h	1	4	8	12	24

[a]This general factorial design gave rise to 45 combinations (3 × 3 × 5). This statistical model, developed from a finite number of experimental runs, can predict the results of a larger superset of possible experiments within the range of SI-ATRP parameters studied.

tethered polymer chains. Obtaining this information is usually not straightforward. Releasing tethered polymer chains from the substrate can introduce impurities and the severed polymers are not always obtained in a quantity that is sufficient for molecular weight determination using size exclusion chromatography (SEC).[30] Precise experimental determination of rate constants neccessitates use of special methods, such as pulsed laser polymerization and electron paramagnetic resonance (EPR),[31,32] which can be difficult to implement. Sometimes, if the experimental estimates of rate constants are unavailable, they are iteratively determined so as to bring the model predictions in line with experimental results.[26]

Nonidealities inherent to the SI-ATRP process further complicate the development of ab initio models. These include confinement effects caused by a high grafting density, gradients in monomer and catalyst concentration and mass transfer limitations.[33] In some cases, the catalysts and the monomer are not equally accessible to all growing chains, resulting a broader CLD for the surface-initiated process as compared to the highly monodisperse molecular weight distribution than is routinely obtained in a solution ATRP process.[34,35] Techniques such as Monte Carlo[36] and Gillespie stochastic simulation algorithm (GSSA)[37,38] simulations that can account for these nonidealities require computationally expensive approaches. Finally, the predictive scope of these models is restricted to CLD alone and does not include other interfacial properties, such as surface charge or wettability.

Because of these limitations, developing a quantitative understanding of the dependence of polymer coating properties on SI-ATRP parameter design through stochastic methods and molecular modeling can be challenging. In contrast, we decided to develop an alternative modeling approach using statistical design of experiments (DOE).

Poly[{2-(methacryloyloxy) ethyl} dimethyl-(3-sulfopropyl) ammonium hydroxide] (PMEDSAH), a zwitterionic polymer brush, undergoes a hydrophilic-to-hydrophobic transition that is governed by brush-specific parameters (e.g., thickness and monodispersity) as well as kinetic features of the polymerization step (e.g., propagation rate during ATRP[39]). To create tailored polymer architectures and tunable CLD for PMEDSAH, we have used surface-initiated atom transfer radical polymerization (SI-ATRP[40]).[41] For PMEDSAH brushes produced by SI-ATRP, Cheng et al.[39] found that thin brushes are usually unassociated and hydrophilic, whereas thick brushes may or may not produce self-associated hydrophobic brushes depending on the propagation rate. If the critical thickness for the hydrophilic-to-hydrophobic transition can be lowered, typically achieved by bringing about low propagation rates in SI-ATRP, unusually thin associated gel architectures can be realized.[39]

PMEDSAH brushes have been identified as promising synthetic substrates for culturing human embryonic stem cells (hESCs) under feeder-free and xeno-free conditions.[42] PMEDSAH coatings can maintain hESC pluripotency in fully defined culture conditions during long-term expansion, thereby circumventing the drawbacks of animal-derived products.[43] Earlier, we reported that hESC proliferation rates are highly sensitive to differences in the gel architecture of PMEDSAH, with a coating possessing a moderate degree of self-association favoring rapid stem cell self-renewal.[44] In Qian et al.,[44] we concluded that the rate of stem cell self-renewal can be increased or decreased by modifying the gel architecture of PMEDSAH. Therefore, the architecture of PMEDSAH brushes is a key design parameter that exerts a substantial influence over the proliferation rate of hESCs cultured for tissue engineering applications. Our work was motivated by the need for a property prediction tool that could guide SI-ATRP parameter selection and enable access to PMEDSAH brushes possessing any desired architecture. We anticipate that accurate prediction of SI-ATRP outcomes will aid the synthesis of PMEDSAH brushes with the optimal properties for facilitating rapid expansion of hESC populations.

In this paper, we report the development of a statistical model that successfully guided the SI-ATRP of PMEDSAH brushes of diverse architectures and functions, including a previously inaccessible polymer brush regime. This predictive model will be more effective in informing experimentalists about reaction conditions for obtaining polymer brushes with desired interfacial properties, compared to conventional trial-and-error approaches.

2. EXPERIMENTAL SECTION

2.1. Chemical Vapor Deposition Polymerization of ATRP Initiator. Using a previously described chemical vapor deposition (CVD) polymerization approach,[45] the initiator coatings were deposited on the substrates in the form of a thin film bearing bromoisobutyryl ester groups for subsequent ATRP initiation. Using Fourier Transformed Infrared (FTIR) spectroscopy, two characteristic bands—the first at 1730 cm^{-1}, indicative of the C═O bond of the ester groups and the second band at 1160 cm^{-1}, which is characteristic of the C−O−C stretches, were used to confirm the chemical structure of the initiator.[45] FTIR spectra can be found in Figure S1. Ellipsometric characterization of the initiator coating was performed as described in Qian et al.[44]

2.2. Experimental Design for SI-ATRP. To conduct a systematic exploration of the experimental space of SI-ATRP, we used a general factorial design with the three design variables set at the levels summarized in Table 1. The design variables form the inputs to our statistical model and the responses (thickness and contact angle) are its outputs. It is important to note that these 45 combinations merely represent a systematic sampling of the infinite combinations possible within the SI-ATRP parameter space. Each of the 45 experimental runs was performed twice. Once a satisfactory statistical model was obtained, it was not necessary to conduct further replicates (the Supporting Information section includes a description of the procedure used for model discrimination and selection of the best statistical model). By analyzing results from this small sample space, we can make predictions about any point in the entire experimental space, including those points about which we have no prior knowledge. The order of experimental runs was randomized to ensure independence of the data points. Details about choosing factors and

DOI: 10.1021/acsami.6b04370
ACS Appl. Mater. Interfaces XXXX, XXX, XXX−XXX

factor levels, statistical diagnostic tests performed for ensuring normality and independence of data obtained, are provided in the Supporting Information section. Experimental results from the systematic sampling were used to construct the statistical model. Other experimental variables, i.e., monomer concentration, solvent composition, ratio of ligand (2,2-bipyridyl) to total copper and reaction temperature were maintained constant throughout the study.

2.3. Procedure for SI-ATRP of MEDSAH. Unless otherwise specified, all the chemicals described in this section were purchased from Sigma-Aldrich and used without further purification. The surface-initiated ATRP of [2-{(methacryloyloxy)ethyl}] dimethyl-(3-sulfopropyl) ammonium hydroxide (MEDSAH) (Monomer Polymer Dajac Laboratories, Trevose, PA) was conducted using the procedure detailed by Qian et al.[44] In brief, the ATRP reaction was allowed to proceed for the desired duration (1, 4, 8, 12, 24 h) under argon atmosphere at 22 °C. Upon completion, substrates were rinsed with 1% sodium chloride solution and deionized water and dried with a jet of nitrogen. The solvent ratio (methanol: water) and the concentration of monomer (0.4 g/mL) was maintained constant for all experiments whereas the molar ratio of copper(I) chloride to monomer and the molar ratio of copper(I) chloride and copper(II) chloride was varied across experiments according to the values specified in the experimental design (Table 1). The number of moles of 2,2 bipyridyl charged was maintained constant at twice the total number of moles of copper(I) chloride and copper(II) chloride.

2.4. Thickness Measurements Using Ellipsometry. Ellipsometry was performed on silicon wafers (Silicon Valley Microelectronics, CA) with a native silicon dioxide layer of 2.5 nm thickness. Coating thickness was measured before and after ATRP with a nulling ellipsometer (EP3 Nanofilm, Accurion GmbH, Germany). Ellipsometric delta and psi values were collected at a wavelength of 531.9 nm. Fixed values were used for the real (n = 1.58) and imaginary (k = 0) components of the refractive index of the polymer coatings. It should be noted that the refractive index of the initiator coating was very close to that of PMEDSAH. After ATRP was completed, the thickness of the PMEDSAH coating formed was calculated by subtracting the initial thickness of the initiator layer from the post-ATRP thickness. Three readings were collected for each substrate and two substrates were used for each experimental run.

2.5. Contact Angle Measurements. Static contact angles of deionized water were measured using a contact angle goniometer (Ramé-Hart 200-F1 goniometer). Measurements were taken at three different locations and averaged for each substrate. Two substrates were used per experimental run.

2.6. Data Analysis Using Analysis of Variance. Analysis of variance (ANOVA) is a statistical inference tool that identifies significant causes of variation—main effects and interactions between experimental factors. ANOVA was performed for thickness and contact angle on Minitab (Minitab Inc., State College, PA) with a 5% level of significance. Model reduction was performed by selecting the significant factor effects identified from the regression ANOVA (Partial sum of squares, type III) and discarding insignificant model terms. Regression analysis was performed using response surface reduced quadratic model on Design Expert 9 software (Stat-ease Inc., Minneapolis, MN).

2.7. Validation Experiments. For every regime of gel architecture, the statistical model was verified by performing validation experiments and comparing their results to predictions. We selected validation points such that they did not overlap with the points used for statistical model construction. Four points were chosen in the design space so that each point would yield coatings belonging to each of the four regimes. All validation runs was replicated to be consistent with the experimental design (n = 2). In total, eight validation experiments were performed to see whether the statistical model equations were successful in predicting thickness and contact angle in the four regimes identified. The point prediction tool of Design Expert 9 (Stat-ease Inc., Minneapolis, MN) was used to generate predictions.

3. RESULTS AND DISCUSSION

We hypothesized that a response surface methodology (RSM)[46,47] will enable determination of the SI-ATRP reaction parameters required to achieve a desired gel architecture. Although RSM is used widely in organic synthesis[48,49] to predict reaction outcomes, this study is, to the best of our knowledge, the first report of an RSM-based study of surface-initiated polymerization. The initial goal was to identify a quantitative relationship between the property space of PMEDSAH coatings and the vast experimental space accessible by SI-ATRP. We implemented a factorial design of experiments (Table 1) to sample the experimental space systematically and analyzed the roles of statistically significant main effects and interactions in determining thickness and wettability. The result was a predictive model that described thickness and contact angle as a function of (i) catalyst quantity, (ii) ratio of activator Cu^{I} to deactivator Cu^{II} species and (iii) reaction time. After a validation phase, the statistical model was employed to guide the synthesis of thin associated brushes, a gel architecture that was discovered to be limited to a narrow experimental region.

3.1. Comparing the Impact of Design Variables on Thickness and Contact Angle. After completing 90 experimental runs (Table 1), the next step was to perform a statistical analysis of the results in order to identify the most significant sources of variation and thereby understand the roles of the three experimental variables on thickness and contact angle. We thus completed two sets of ANOVA analysis for thickness and contact angle. ANOVA yields F-ratios, which forms the basis for rank-ordering main effects and understanding their relative importance. Apart from quantifying the impact of the three main effects on each response, ANOVA is well-suited to identifying statistically significant two-factor and three-factor interactions. In Table 2, polymer brush thickness is found to be significantly influenced by all parameters studied (all p-values are below 1×10^{-3}). The ANOVA analysis identifies reaction time, followed by catalyst ratio, as the lead parameters with the highest impact. In the range of catalyst quantity studied (1−3 mol %), thickness does not appear to be particularly sensitive to catalyst quantity. However, catalyst quantity has a strong interaction (AB) with catalyst ratio. In contrast, the ANOVA analysis for contact angle (Table 3) presents a completely different picture, with catalyst quantity identified as the clearly dominant factor. The higher the

Table 2. Summary of ANOVA Results for Thickness[a]

source of variation	sum of squares	degrees of freedom	mean square	F_0	p-value
cat. qty (A)	1536.0	2	768.0	15.6	$< 1 \times 10^{-3}$
cat. ratio (B)	19489.2	2	9744.6	198.1	$< 1 \times 10^{-3}$
time (C)	57124.6	4	14281.2	290.4	$< 1 \times 10^{-3}$
AB	4260.8	4	1065.2	21.6	$< 1 \times 10^{-3}$
AC	1946.8	8	243.4	4.9	$< 1 \times 10^{-3}$
BC	3432.7	8	429.0	8.7	$< 1 \times 10^{-3}$
ABC	6623.0	16	413.9	8.4	$< 1 \times 10^{-3}$
error	2212.9	45	49.2		
total	96626.1	89	1085.7		

[a]The tabulated values of the F-test statistic help identifying the principal sources of variation in thickness, with higher F-ratios implying a greater contribution. Here, catalyst ratio and reaction time are the two most significant factors.

DOI: 10.1021/acsami.6b04370
ACS Appl. Mater. Interfaces XXXX, XXX, XXX−XXX

Table 3. Summary of ANOVA Analysis for Contact Angles[a]

source of variation	sum of squares	degrees of freedom	mean square	F_0	p-value
cat. qty (A)	7195.9	2	3598.0	90.9	$<1 \times 10^{-3}$
cat. ratio (B)	1511.0	2	755.5	19.1	$<1 \times 10^{-3}$
time (C)	10826.4	4	2706.6	68.4	$<1 \times 10^{-3}$
AB	939.3	4	234.8	5.9	0.001
AC	5092.2	8	636.5	16.1	$<1 \times 10^{-3}$
BC	1289.3	8	161.2	4.1	0.001
ABC	1151.7	16	72.0	1.8	0.059
error	1781.8	45	39.6		
total	29787.6	89	3598.0		

[a]Unlike in the film thickness model, the catalyst quantity dominates the statistical model for contact angles. Reaction time is prominent both, as a stand-alone effect and because of its interaction with catalyst quantity.

quantity of catalyst, the more hydrophobic are the resulting coatings. Interestingly, catalyst quantity was even more relevant than reaction time, which also favored higher contact angles. Catalyst ratio, however, only marginally influences contact angle, a finding that contrasts with the strong effect of catalyst ratio on thickness. Among the interaction terms, the interaction between reaction time and catalyst quantity is most significant (AC).

Predictive models for thickness and contact angle were constructed using regression analysis, as described in sections 4 and 5 of the Supporting Information. Two equations, each describing thickness and contact angle as functions of significant model terms, were obtained. These include main effects and interaction terms. The statistical model equations are depicted graphically in the form of response surface plots as shown in Figure 1. These 3D surface plots are complete representations of the effects of all three experimental variables and their interactions.

3.2. Prediction of Four Regimes of Gel Architecture. The contact angle and thickness results obtained from the 90 experimental runs were plotted in the form of a scatter plot (Figure 2A) and then segmented into four quadrants (Figure 2B), as described below. The thickness ranged from 2.5 to 140.5 nm. Coatings thicker than 70 nm (median value) were classified as thick and those below 70 nm were denoted thin.

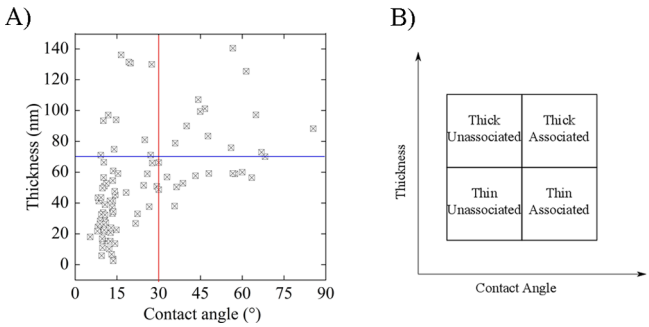

Figure 2. (A) Scatter plot of thickness versus contact angle. The data were classified into four regimes by setting boundaries of 70 nm (horizontal blue line) for thickness and 30° (vertical red line) for contact angle. (B) Quadrants representing four regimes of gel architecture, as identified from the scatter plot.

For segmenting contact angle data, we have to consider zwitterionic self-association[39,50−52] of PMEDSAH, which causes an increase in contact angle in proportion to the degree of self-association. Consistent with previous studies,[39,51] contact angles less than 30° were considered to belong to the hydrophilic and unassociated regime, those greater than 30° fall within the self-associated regime.[39,51] Therefore, the data can be grouped into four regimes: thick associated, thick unassociated, thin unassociated, and thin associated.

From the scatter plot in Figure 2A, we deduced that there exists a weak overall correlation (R^2 = 0.514) between contact angle and thickness. In the thick associated regime and the thin unassociated regime alone, where the thickness-dependent behavior of contact angle is evident, the correlation between the hydrophobicity of the coatings and its thickness is very strong. However, if we consider the data points in the thick unassociated regime and the thin associated regime alone, this correlation does not hold and thickness and contact angle are independent of each other. On the basis of this analysis, it appears that the relationship between PMEDSAH's thickness and its degree of self-association is regime-dependent and complex.

3.3. Assessment and Validation of the Predictive Character of the Statistical Model. By simultaneously solving model equations for thickness and contact angle, it should be possible to experimentally access arbitrary combina-

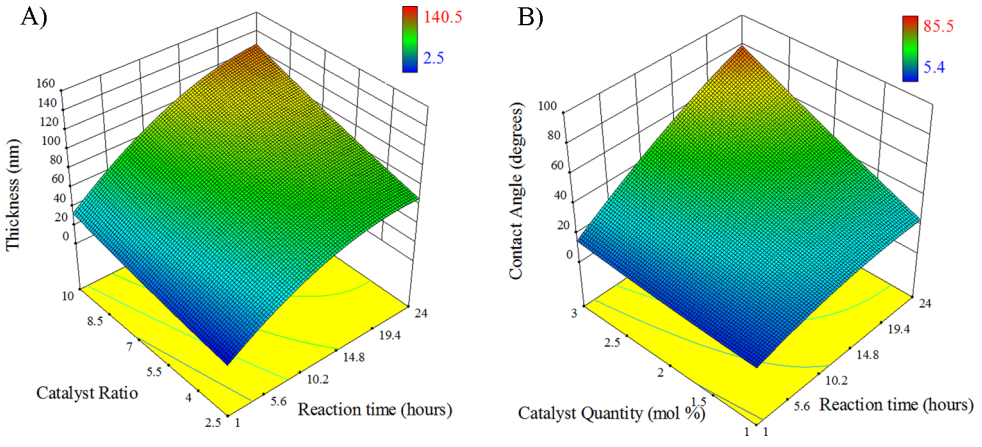

Figure 1. (A) Three-dimensional surface plot predicting film thickness as a function of catalyst ratio and reaction time at 1.5 mol % catalyst quantity. The statistical model that this plot represents, can predict thickness across all possible experiments that can be performed within the studied range. (B) Three-dimensional surface plot predicting film contact angle as a function of catalyst quantity and reaction time at a catalyst ratio of 9.

DOI: 10.1021/acsami.6b04370
ACS Appl. Mater. Interfaces XXXX, XXX, XXX−XXX

tions of contact angle and thickness, thereby realizing the desired gel architecture. As an example, if we wish to synthesize a thin associated brush architecture with a target thickness of 70 nm and a target contact angle of 45°, we would have to employ the following ATRP conditions: catalyst quantity of 3 mol %, catalyst ratio of 9 and a reaction time of 10 h, as suggested by the simultaneous solution of thickness and contact angle model equations. In Figure 3, experimental values were plotted against

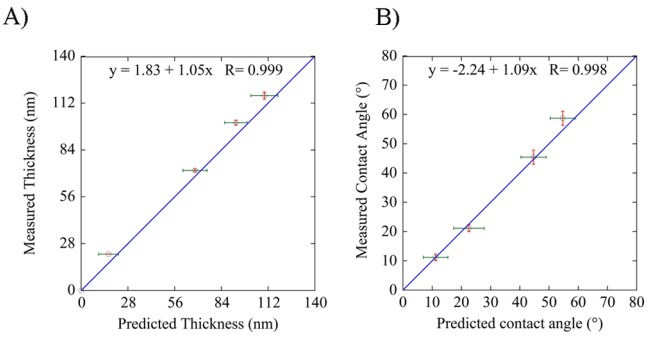

Figure 3. Comparison of experimental and predicted values (hollow circles) for (A) thickness and (B) contact angle. Horizontal error bars in green indicate 95% confidence interval of the statistical model prediction, whereas vertical error bars in red represent standard deviation of experimental measurement. The blue line is a reference representing an ideal agreement between predicted and measured values ($y = x$).

predicted values for each regime. We found that the experimental results correlate well with statistical model predictions in all four regimes.

3.4. Identifying a Design Space for the Thin Associated Regime. In Figure 2A, we observed prominent differences of the population density in the four regimes, with the thin unassociated regime being the most densely populated and the thick unassociated and the thin associated regimes the most sparsely populated. This suggests that the thin unassociated regime is the easiest brush architecture to obtain experimentally, whereas it is feasible to obtain the thick unassociated and the thin associated regimes only within narrow regions. This observation raises the following question: Can our statistical model identify experimental boundaries, within which a given gel architecture can be obtained reliably? If so, does this hold even for atypical brushes such as thin and associated brushes? In Figure 4, regions of experimental viability predicted for thin associated brushes have been represented graphically. Model equations for contact angle and thickness were solved simultaneously to yield a design space where thickness will be 70 nm or less and contact angle 30° or greater. At a catalyst concentration of 1.5 mol % and below, no solution exists, indicating that it is unfeasible to produce thin associated brushes at low catalyst concentrations. As we increase the catalyst quantity to 2 mol % and higher, the solution space widens, attaining a maximum area at 3 mol % catalyst quantity. Similar plots for thick associated brushes and thick unassociated brushes and a brief discussion of their design spaces are included in Figure S6.

3.5. Reaction Time and Catalyst Ratio Dominate Film Thickness. From the ANOVA analysis, we established that all three main effects (reaction time, catalyst quantity and catalyst ratio) were significant in determining thickness. The individual impact of each effect can be pictured as protagonistic or antagonistic depending on whether the slope of the plot in Figure 5 is positive or negative. Reaction time had the highest

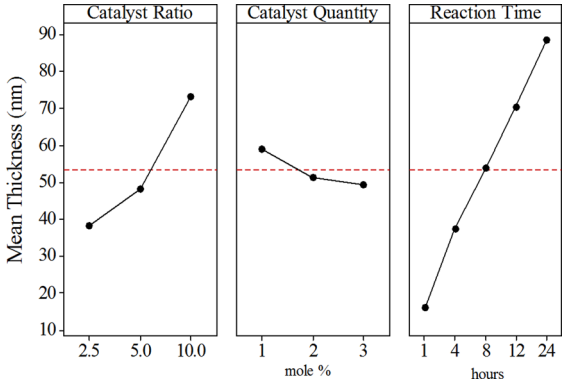

Figure 5. Main effects on thickness. From left to right, the effects of catalyst ratio, catalyst quantity and reaction time on thickness are plotted. The red dotted line refers to the location of the overall mean thickness (53.4 nm) of all 90 data points. By comparing slopes, we can see that reaction time and catalyst ratio have the strongest effects on thickness. The effect of catalyst quantity is less pronounced.

slope, with thickness growing linearly with increasing reaction time. With time, more monomer is added to the growing PMEDSAH chain, resulting in a linear increase of thickness with time. The rate of increase of thickness with time is controlled by the catalyst ratio. Increasing the initial quantity of the activating Cu^{I} relative to the deactivating Cu^{II} will affect the equilibrium position of the activation−deactivation step.[53]

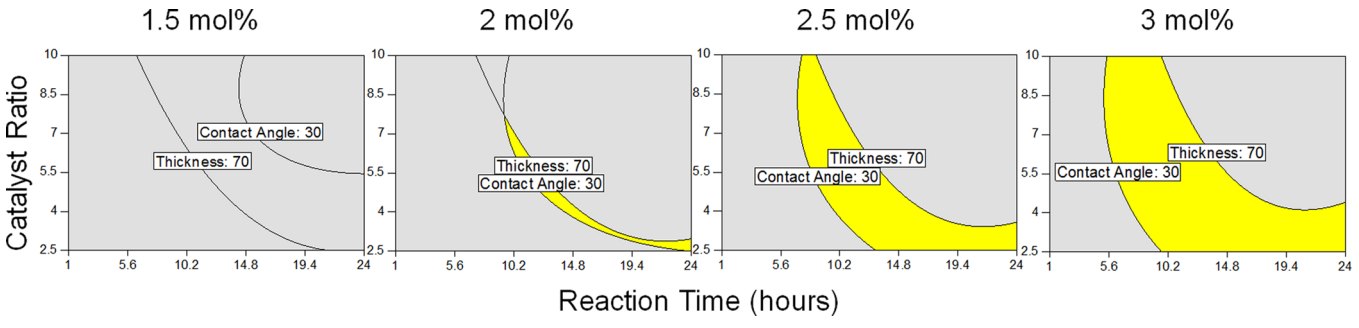

Figure 4. Design space for thin associated brushes across different catalyst quantities (in mol %). The yellow regions represent the experimental boundaries within which it is possible to obtain coatings belonging to this regime of gel architecture. The design space was obtained by simultaneous solution of statistical model equations to yield operating conditions which will lead to thickness less than 70 nm and contact angle greater than 30°. These plots show how the experimentally accessible space becomes larger with increasing catalyst quantity.

DOI: 10.1021/acsami.6b04370
ACS Appl. Mater. Interfaces XXXX, XXX, XXX−XXX

Thus, for the same reaction time, thicker coatings are obtained for a higher ratio of Cu^{I} to Cu^{II}. The effect of catalyst quantity on thickness, though statistically significant (Table 2), was less pronounced and had the lowest F-ratio among the three main effects. Unlike the other two effects, it was observed to have an antagonistic effect on thickness, with a slight decrease in thickness observed upon increasing catalyst quantity (Figure 5). According to SI-ATRP kinetic models, the time-evolution of chain length distribution is expected to depend only on the catalyst ratio and not on the catalyst quantity. The migration-termination hypothesis[29] has explained the departure of these experimental trends from SI-ATRP kinetic models. Among two-factor interaction terms, the interaction AB between catalyst quantity and catalyst ratio was the most relevant (Table 2, AB interaction, *p*-value less than 0.001). Figure 6

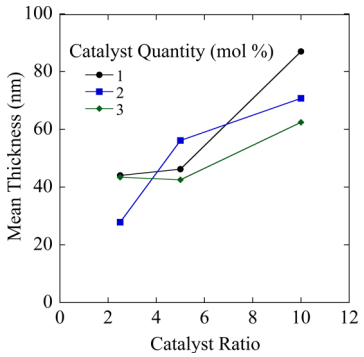

Figure 6. Interaction plot for thickness. The increase in thickness with catalyst ratio is dependent on the catalyst quantity.

indicates that the sensitivity of thickness to catalyst ratio is lowered, when a high catalyst quantity is employed, whereas thickness is highly correlated with catalyst ratio at low levels of catalyst quantity. Interestingly, the interdependence of catalyst quantity and catalyst ratio suggests that they operate in tandem rather than independently.

3.6. Hydrophilic-to-Hydrophobic Transition Is Controlled by Catalyst Quantity. The four regimes of gel architecture differ clearly in the degree of correlation between thickness and contact angle, with high correlation in the thick associated and thin unassociated regimes and none in the thick unassociated and thin associated regimes. In spite of possessing a lower mean brush thickness than the thick associated regime, the polymer brushes in the thin associated regime still exhibit a high degree of association, with contact angles comparable to those of the thick associated regime. Second, although thick unassociated brushes are much thicker than thin unassociated brushes, they remain unassociated and are as hydrophilic as those in the thin unassociated regime. This anomalous behavior of brushes belonging to the thick unassociated and thin associated regimes indicates that a high thickness is not a necessary condition for forming association in zwitterionic polymer brushes. It is well established that PMEDSAH undergoes a transition from its original hydrophilic state to a hydrophobic brush as a consequence of zwitterionic self-association.[51,52,54] Water is excluded from the brush due to the formation of interchain and intrachain association between the quaternary ammonium cation and sulfonate anion of adjacent side chains[39] (Figure 7). Thicker brushes are likely to have increased chain association and thus exclude more water from the brush, explaining the increase of contact angle with reaction

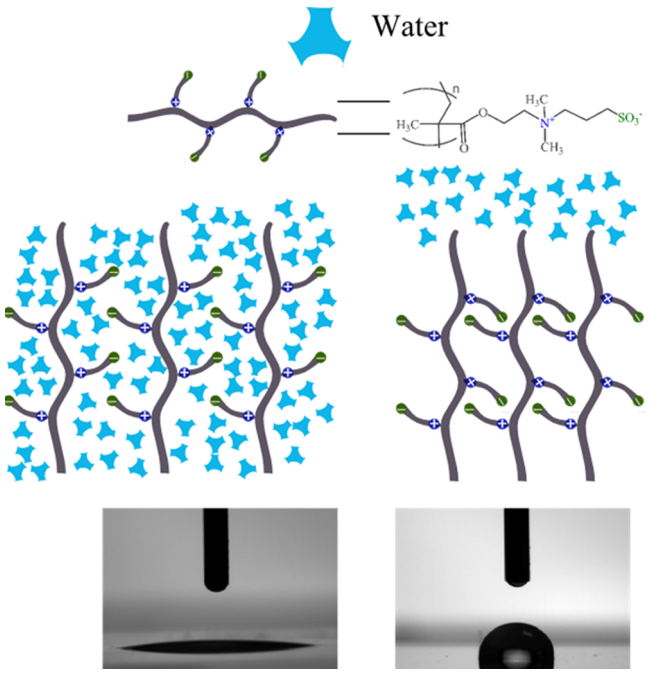

Figure 7. Wettability transition of PMEDSAH from hydrophilic to hydrophobic. The schematic represents the architecture of a PMEDSAH brush and its interaction with water when it is unassociated and when it undergoes hydrophobic collapse because of zwitterionic self-association. Images of representative water droplets illustrate the wettability differences.

time. What is surprising is that the catalyst quantity variable, which had only a slightly negative effect on thickness, is the most powerful factor in the contact angle model. Considering the slopes of the main effects plots for contact angle (Figure 8)

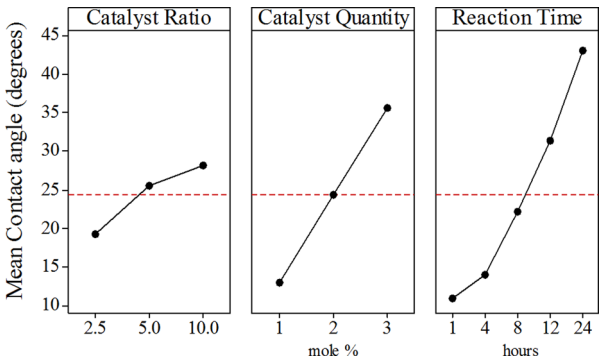

Figure 8. Main effects on contact angle. From left to right, the effects of catalyst ratio, catalyst quantity, and reaction time on contact angle are plotted. The red dotted line refers to the overall average contact angle (24°) of all 90 data points. From the slopes, we can conclude that catalyst quantity and reaction time exert the most prominent effect on contact angle.

and thickness (Figure 5), catalyst quantity has a positive slope in Figure 8, whereas it has a negative slope in Figure 5. Moreover, catalyst quantity is highly influential not only as a standalone effect, but also in its interaction with reaction time, which has the highest *F*-ratio among all interaction terms in the contact angle model. The interaction plot for contact angle is shown in Figure 9, where the contact angle increases rapidly with reaction time at high catalyst quantity, whereas it remains unaffected by reaction time at low catalyst quantity. Therefore,

DOI: 10.1021/acsami.6b04370
ACS Appl. Mater. Interfaces XXXX, XXX, XXX−XXX

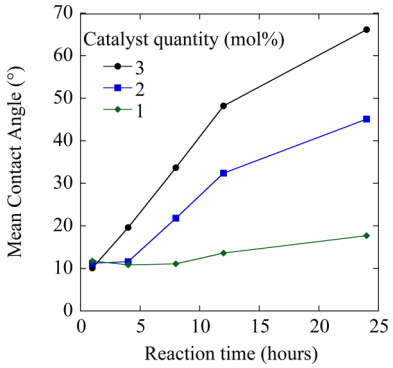

Figure 9. Interaction plot for contact angle. The level of catalyst quantity employed determines the dependence of contact angle on reaction time. At a higher catalyst quantity, the contact angle becomes more dependent on reaction time.

the sensitivity of contact angle to reaction time is governed by the level of catalyst quantity employed. To understand these findings, it is helpful to refer to the study performed by Cheng et al.[39] The authors noted that the self-association of PMEDSAH is driven by two factors: the thickness of the brush as well as the monodispersity of the CLD. In a monodisperse brush, the critical thickness required to trigger self-association is lower than it would be for a polydisperse brush. Exploring only 6 combinations of catalyst quantity and catalyst ratio, Cheng et al.[39] reported that that decreasing the ratio of activator to deactivator (Cu^{I}:Cu^{II}) would reduce the critical thickness by improving monodispersity. However, this study not explored the effects of catalyst quantity as exhaustively and systematically. From our statistical models, we established that catalyst ratio, albeit an important determinant of thickness, has only a marginal role in determining contact angle. Hence we propose that the critical thickness at which zwitterionic association causes wettability changes is controlled by catalyst quantity and not by catalyst ratio.

3.7. Physical Validity of the Statistical Model and Potential Uses for hESC Culture. In all four validation tests, the experimental results for thickness and contact angle were within the predicted range. Therefore, this statistical model can be considered a valid mathematical representation of the SI-ATRP process and employed as a predictive tool to obtain PMEDSAH coatings of the desired gel architecture. In ref 44, we reported that PMEDSAH's capacity for facilitating hESC self-renewal could be tuned by modifying the gel architecture. We had studied three coatings: two belonging to the thick associated regime and one to the thin unassociated regime. Even though they all had similar surface charge and roughness, the thick associated coating with a moderate degree of association was found to have higher hESC propagation rates. Using the predictive tool established in this paper, we can now access coatings from the yet unevaluated thick unassociated and thin associated regimes, perform hESC culture studies using these coatings, and discover whether higher or lower rates of hESC expansion result.

4. CONCLUSIONS

We quantified the dependence of brush thickness and wettability on key SI-ATRP parameters by constructing and validating a statistical model that simultaneously predicted the thickness−time trajectory as well as the degree of zwitterionic self-association. Our model indicates that we can reduce the critical thickness at which self-association triggers wettability changes by increasing the catalyst quantity. This provides reliable polymerization conditions to synthesize coatings with unusual gel architectures, such as thin associated brushes. Because our model is constructed from empirical results of systematically designed experiments, we did not require any simplifying assumptions. Moreover, as a property prediction tool, DOE, unlike ab initio modeling, can be used to model a range of coating properties. We further developed a quantitative relationship between the properties of PMEDSAH brushes and SI-ATRP parameters. This predictive tool provides on-demand access to PMEDSAH brushes for four regimes of gel architecture. Because our modeling approach can predict the outcomes of SIP accurately, it can be extended to other SIP systems to discover, design, and identify unusual combinations of polymer brush attributes.

■ ASSOCIATED CONTENT

Supporting Information

The Supporting Information is available free of charge on the ACS Publications website at DOI: 10.1021/acsami.6b04370.

Complete information about experimental design model development, brush characterization, and diagnostic tests of normality and independence; atom force microscopy evaluation of surface roughness, Fourier-transformed infrared spectroscopy (FTIR) data, and raw data sets from the DOE are also provided (PDF)

■ AUTHOR INFORMATION

Corresponding Author

*E-mail: lahann@umich.edu. Phone: +173 4763 7543.

Notes

The authors declare no competing financial interest.

■ ACKNOWLEDGMENTS

We acknowledge the Defense Threat Reduction Agency (DTRA) for funding provided through Grant HDTRA1-12-1-0039 as a part of the interfacial dynamics and reactivity program. We further acknowledge support from the Army Research Office (ARO) under Grant W911NF-11-1-0251. We thank Prof. Anish Tuteja for access to the contact angle goniometer. Prof. Vijay Nair is gratefully acknowledged for sharing his valuable insights on statistical modeling.

■ REFERENCES

(1) Stuart, M. A. C.; Huck, W. T. S.; Genzer, J.; Muller, M.; Ober, C.; Stamm, M.; Sukhorukov, G. B.; Szleifer, I.; Tsukruk, V. V.; Urban, M.; Winnik, F.; Zauscher, S.; Luzinov, I.; Minko, S. Emerging Applications of Stimuli-responsive Polymer Materials. *Nat. Mater.* **2010**, *9*, 101−113.

(2) Zhou, F.; Hu, H.; Yu, B.; Osborne, V. L.; Huck, W. T. S.; Liu, W. Probing the Responsive Behavior of Polyelectrolyte Brushes Using Electrochemical Impedance Spectroscopy. *Anal. Chem.* **2007**, *79*, 176−182.

(3) Zhou, F.; Biesheuvel, P. M.; Choi, E.-Y.; Shu, W.; Poetes, R.; Steiner, U.; Huck, W. T. S. Polyelectrolyte Brush Amplified Electroactuation of Microcantilevers. *Nano Lett.* **2008**, *8*, 725−730.

(4) Comrie, J. E.; Huck, W. T. S. Exploring Actuation and Mechanotransduction Properties of Polymer Brushes. *Macromol. Rapid Commun.* **2008**, *29*, 539−546.

DOI: 10.1021/acsami.6b04370
ACS Appl. Mater. Interfaces XXXX, XXX, XXX−XXX

(5) Zhou, F.; Shu, W.; Welland, M. E.; Huck, W. T. S. Highly Reversible and Multi-Stage Cantilever Actuation Driven by Polyelectrolyte Brushes. *J. Am. Chem. Soc.* **2006**, *128*, 5326−5327.
(6) Azzaroni, O.; Brown, A. A.; Huck, W. T. S. Tunable Wettability by Clicking Counterions Into Polyelectrolyte Brushes. *Adv. Mater.* **2007**, *19*, 151−154.
(7) Zhang, Z.; Chen, S.; Chang, Y.; Jiang, S. Surface Grafted Sulfobetaine Polymers via Atom Transfer Radical Polymerization as Superlow Fouling Coatings. *J. Phys. Chem. B* **2006**, *110*, 10799−10804.
(8) Cheng, G.; Li, G.; Xue, H.; Chen, S.; Bryers, J. D.; Jiang, S. Zwitterionic Carboxybetaine Polymer Surfaces and their Resistance to Long-term Biofilm Formation. *Biomaterials* **2009**, *30*, 5234−5240.
(9) Yuan, S. J.; Pehkonen, S. O.; Ting, Y. P.; Neoh, K. G.; Kang, E. T. Antibacterial Inorganic-Organic Hybrid Coatings on Stainless Steel via Consecutive Surface-Initiated Atom Transfer Radical Polymerization for Biocorrosion Prevention. *Langmuir* **2010**, *26*, 6728−6736.
(10) Welch, M.; Rastogi, A.; Ober, C. Polymer Brushes for Electrochemical Biosensors. *Soft Matter* **2011**, *7*, 297−302.
(11) Uhlmann, P.; Merlitz, H.; Sommer, J.-U.; Stamm, M. Polymer Brushes for Surface Tuning. *Macromol. Rapid Commun.* **2009**, *30*, 732−740.
(12) Azzaroni, O. Polymer Brushes Here, There, and Everywhere: Recent Advances in their Practical Applications and Emerging Ppportunities in Multiple Research Fields. *J. Polym. Sci., Part A: Polym. Chem.* **2012**, *50*, 3225−3258.
(13) Hawker, C. J.; Bosman, A. W.; Harth, E. New Polymer Synthesis by Nitroxide Mediated Living Radical Polymerizations. *Chem. Rev.* **2001**, *101*, 3661−3688.
(14) Barner-Kowollik, C.; Davis, T. P.; Heuts, J. P. A.; Stenzel, M. H.; Vana, P.; Whittaker, M. RAFTing Down Under: Tales of Missing Radicals, Fancy Architectures, and Mysterious Holes. *J. Polym. Sci., Part A: Polym. Chem.* **2003**, *41*, 365−375.
(15) Baum, M.; Brittain, W. J. Synthesis of Polymer Brushes on Silicate Substrates via Reversible Addition Fragmentation Chain Transfer Technique. *Macromolecules* **2002**, *35*, 610−615.
(16) Pyun, J.; Kowalewski, T.; Matyjaszewski, K. Synthesis of Polymer Brushes Using Atom Transfer Radical Polymerization. *Macromol. Rapid Commun.* **2003**, *24*, 1043−1059.
(17) Barbey, R.; Lavanant, L.; Paripovic, D.; Schüwer, N.; Sugnaux, C.; Tugulu, S.; Klok, H.-A. Polymer Brushes via Surface-Initiated Controlled Radical Polymerization: Synthesis, Characterization, Properties, and Applications. *Chem. Rev.* **2009**, *109*, 5437−5527.
(18) Krishnamoorthy, M.; Hakobyan, S.; Ramstedt, M.; Gautrot, J. E. Surface-Initiated Polymer Brushes in the Biomedical Field: Applications in Membrane Science, Biosensing, Cell Culture, Regenerative Medicine and Antibacterial Coatings. *Chem. Rev.* **2014**, *114*, 10976−11026.
(19) Mansfeld, U.; Pietsch, C.; Hoogenboom, R.; Becer, C. R.; Schubert, U. S. Clickable Initiators, Monomers and Polymers in Controlled Radical Polymerizations - a Prospective Combination in Polymer Science. *Polym. Chem.* **2010**, *1*, 1560−1598.
(20) Jeyaprakash, J. D.; Samuel, S.; Dhamodharan, R.; Rühe, J. Polymer Brushes via ATRP: Role of Activator and Deactivator in the Surface-initiated ATRP of Styrene on Planar Substrates. *Macromol. Rapid Commun.* **2002**, *23*, 277−281.
(21) Rodda, A. E.; Ercole, F.; Nisbet, D. R.; Forsythe, J. S.; Meagher, L. Optimization of Aqueous SI-ATRP Grafting of Poly(Oligo-(Ethylene Glycol) Methacrylate) Brushes from Benzyl Chloride Macroinitiator Surfaces. *Macromol. Biosci.* **2015**, *15*, 799−811.
(22) Czitrom, V. One-Factor-at-a-Time versus Designed Experiments. *Am. Stat.* **1999**, *53*, 126−131.
(23) Siegwart, D. J.; Leiendecker, M.; Langer, R.; Anderson, D. G. Automated ARGET ATRP Accelerates Catalyst Optimization for the Synthesis of Thiol-functionalized Polymers. *Macromolecules* **2012**, *45*, 1254−1261.
(24) Toloza Porras, C.; D'hooge, D. R.; Reyniers, M.-F.; Marin, G. B. Computer-Aided Optimization of Conditions for Fast and Controlled ICAR ATRP of n-Butyl Acrylate. *Macromol. Theory Simul.* **2013**, *22*, 136−149.
(25) Limpoco, F. T.; Bailey, R. C. Real-Time Monitoring of Surface-Initiated Atom Transfer Radical Polymerization Using Silicon Photonic Microring Resonators: Implications for Combinatorial Screening of Polymer Brush Growth Conditions. *J. Am. Chem. Soc.* **2011**, *133*, 14864−14867.
(26) Bain, E. D.; Turgman-Cohen, S.; Genzer, J. Progress in Computer Simulation of Bulk, Confined, and Surface-initiated Polymerizations. *Macromol. Theory Simul.* **2013**, *22*, 8−30.
(27) Gao, X.; Feng, W.; Zhu, S.; Sheardown, H.; Brash, J. L. Kinetic Modeling of Surface-Initiated Atom Transfer Radical Polymerization. *Macromol. React. Eng.* **2010**, *4*, 235−250.
(28) Xiao, D.; Wirth, M. J. Wirth, Kinetics of Surface-Initiated Atom Transfer Radical Polymerization of Acrylamide on Silica. *Macromolecules* **2002**, *35*, 2919−2925.
(29) Zhou, D.; Gao, X.; Wang, W. J.; Zhu, S. Termination of Surface Radicals and Kinetic Modeling of ATRP Grafting from Flat Surfaces by Addition of Deactivator. *Macromolecules* **2012**, *45*, 1198−1208.
(30) Kang, C.; Crockett, R. M.; Spencer, N. D. Molecular-Weight Determination of Polymer Brushes Generated by SI-ATRP on Flat Surfaces. *Macromolecules* **2014**, *47*, 269−275.
(31) Barner-Kowollik, C.; Buback, M.; Egorov, M.; Fukuda, T.; Goto, A.; Olaj, O. F.; Russell, G. T.; Vana, P.; Yamada, B.; Zetterlund, P. B. Critically Evaluated Termination Rate Coefficients for Free-radical Polymerization: Experimental Methods. *Prog. Polym. Sci.* **2005**, *30*, 605−643.
(32) Barner-Kowollik, C.; Beuermann, S.; Buback, M.; Castignolles, P.; Charleux, B.; Coote, M. L.; Hutchinson, R. A.; Junkers, T.; Lacik, I.; Russell, G. T.; Stach, M.; van Herk, A. M. Critically Evaluated Rate Coefficients in Radical Polymerization - 7. Secondary-radical Propagation Rate Coefficients for Methyl Acrylate in the Bulk. *Polym. Chem.* **2014**, *5*, 204−212.
(33) Kim, J.-B.; Huang, W.; Miller, M. D.; Baker, G. L.; Bruening, M. L. Kinetics of Surface-initiated Atom Transfer Radical Polymerization. *J. Polym. Sci., Part A: Polym. Chem.* **2003**, *41*, 386−394.
(34) Prucker, O.; Rühe, J. Mechanism of Radical Chain Polymerizations Initiated by Azo Compounds Covalently Bound to the Surface of Spherical Particles. *Macromolecules* **1998**, *31*, 602−613.
(35) Martinez, A. P.; Carrillo, J.-M. Y.; Dobrynin, A. V.; Adamson, D. H. Distribution of Chains in Polymer Brushes Produced by a Grafting From Mechanism. *Macromolecules* **2016**, *49*, 547.
(36) Milchev, A.; Wittmer, J. P.; Landau, D. P. Formation and Equilibrium Properties of Living Polymer Brushes. *J. Chem. Phys.* **2000**, *112*, 1606−1615.
(37) Gillespie, D. T. A General Method for Numerically Simulating the Stochastic Time Evolution of Coupled Chemical Reactions. *J. Comput. Phys.* **1976**, *22*, 403−434.
(38) Gillespie, D. T. Exact Stochastic Simulation of Coupled Chemical Reactions. *J. Phys. Chem.* **1977**, *81*, 2340−2361.
(39) Cheng, N.; Brown, A. A.; Azzaroni, O.; Huck, W. T. S. Thickness-Dependent Properties of Polyzwitterionic Brushes. *Macromolecules* **2008**, *41*, 6317−6321.
(40) Huang, X.; Wirth, M. J. Surface Initiation of Living Radical Polymerization for Growth of Tethered Chains of Low Polydispersity. *Macromolecules* **1999**, *32*, 1694−1696.
(41) Liu, P.; Domingue, E.; Ayers, D. C.; Song, J. Modification of Ti6Al4V Substrates with Well-defined Zwitterionic Polysulfobetaine Brushes for Improved Surface Mineralization. *ACS Appl. Mater. Interfaces* **2014**, *6*, 7141−7152.
(42) Villa-Diaz, L. G.; Nandivada, H.; Ding, J.; Nogueira-de Souza, N. C.; Krebsbach, P. H.; O'Shea, K. S.; Lahann, J.; Smith, G. D. Synthetic Polymer Coatings for Long-term Growth of Human Embryonic Stem Cells. *Nat. Biotechnol.* **2010**, *28*, 581−583.
(43) Villa-Diaz, L.; Ross, A.; Lahann, J.; Krebsbach, P. Concise Review: The Evolution of Human Pluripotent Stem Cell Culture: From Feeder Cells to Synthetic Coatings. *Stem Cells* **2013**, *31*, 1−7.
(44) Qian, X.; Villa-Diaz, L. G.; Kumar, R.; Lahann, J.; Krebsbach, P. H. Enhancement of the Propagation of Human Embryonic Stem Cells by Modifications in the Gel Architecture of PMEDSAH Polymer Coatings. *Biomaterials* **2014**, *35*, 9581−9590.

DOI: 10.1021/acsami.6b04370
ACS Appl. Mater. Interfaces XXXX, XXX, XXX−XXX

(45) Jiang, X.; Chen, H.-Y.; Galvan, G.; Yoshida, M.; Lahann, J. Vapor-Based Initiator Coatings for Atom Transfer Radical Polymerization. *Adv. Funct. Mater.* **2008**, *18*, 27−35.
(46) Ferdosian, F.; Yuan, Z.; Anderson, M.; Xu, C. C. Synthesis of Lignin-based Epoxy resins: Optimization of Reaction Parameters using Response Surface Methodology. *RSC Adv.* **2014**, *4*, 31745−31753.
(47) Kaith, B. S.; Sharma, R.; Kalia, S.; Bhatti, M. S. Response Surface Methodology and Optimized Synthesis of Guar Gum-based Hydrogels with Enhanced Swelling Capacity. *RSC Adv.* **2014**, *4*, 40339−40344.
(48) Deming, S. N.; Morgan, S. L. *Experimental Design: A Chemometric Approach*; Elsevier: Amsterdam, 1987.
(49) Bess, E. N.; Bischoff, A. J.; Sigman, M. S. Designer Substrate Library for Quantitative, Predictive Modeling of Reaction Performance. *Proc. Natl. Acad. Sci. U. S. A.* **2014**, *111*, 14698−14703.
(50) Monroy Soto, V. M; Galin, J. C. Poly(sulphopropylbetaines): 2. Dilute Solution Properties. *Polymer* **1984**, *25*, 254−262.
(51) Azzaroni, O.; Brown, A. A.; Huck, W. T. S. UCST Wetting Transitions of Polyzwitterionic Brushes Driven by Self-association. *Angew. Chem., Int. Ed.* **2006**, *45*, 1770−1774.
(52) Rubinstein, M.; Dobrynin, A. V. Associations Leading to Formation of Reversible Networks and Gels. *Curr. Opin. Colloid Interface Sci.* **1999**, *4*, 83−87.
(53) Shipp, D. A.; Matyjaszewski, K. Kinetic Analysis of Controlled/Living Radical Polymerizations by Simulations. 2. Apparent External Orders of Reactants in Atom Transfer Radical Polymerization. *Macromolecules* **2000**, *33*, 1553−1559.
(54) Schulz, D. N.; Peiffer, D. G.; Agarwal, P. K.; Larabee, J.; Kaladas, J. J.; Soni, L.; Handwerker, B.; Garner, R. T. Phase Behaviour and Solution Properties of Sulphobetaine Polymers. *Polymer* **1986**, *27*, 1734−1742.

DOI: 10.1021/acsami.6b04370
ACS Appl. Mater. Interfaces XXXX, XXX, XXX−XXX